# Nonlinear acoustic metasurface for simultaneous higher-harmonic generation and demultiplexing

Zhenkun Lin*, Yuning Zhang*, K. W. Wang, and Serife Tol

Department of Mechanical Engineering, University of Michigan, Ann Arbor, MI, USA, 48109-2125

## ABSTRACT

Recently, acoustic/elastic metasurfaces have gained increasing research interests due to their ability to control waves with compact and lightweight structures. A metasurface is a thin layer in the host medium composed of an array of subwavelength-scaled patterns, which introduces an abrupt phase shift in the wave propagation path and tailors wavefront based on generalized Snell's law. The existing metasurfaces mainly depend on the linear dynamic behavior of the structures, while their nonlinear features have not been studied extensively. A couple recent attempts have shown means of introducing nonlinearity in acoustic metasurface designs, resulting in nonlinear effects such as second-harmonic generation (SHG). However, these studies mainly focus on generating and maximizing the higher-order harmonics, while the phase modulation and wavefront tailoring capability are less explored. Our study advances the state of the art and proposes a novel acoustic metasurface design with locally resonant nonlinear elements in the form of curved beams. We explore the nonlinear phenomenon, specifically SHG, of the proposed system using both analytical and numerical frameworks. Our results show that the proposed nonlinear metasurface can achieve SHG in the transmitted acoustic wavefield, and simultaneously demultiplex for different frequency components (i.e., split the second-harmonic component from the fundamental frequency component) by steering them into different directions. This study presents new theoretical and numerical platforms to explore the amplitude-dependent behavior of acoustic metasurfaces, expands their wavefront tailoring capabilities and functionalities, and develops new potentials towards efficient technologies to manipulate acoustic waves.

**Keywords:** Nonlinear acoustic metasurface, second-harmonic generation, acoustic wave demultiplexing

## 1. INTRODUCTION

Acoustic/elastic metamaterials (MMs) and phononic crystals (PCs), consisting of periodically arranged modules, have gained increasing research interests due to their unique properties such as engineered bandgap and effective negative parameters.[1,2] These engineered structural and material systems exhibit intriguing system dynamic properties due to the Bragg scattering and locally resonant effects, leading to diverse applications including energy harvesting systems,[3,4] vibration suppression devices,[5,6] and mechanical topological insulators.[7] Moreover, their nonlinear behaviors have been explored, offering diverse nonlinear phenomena such as supratransmission,[8,9] non-reciprocal wave propagation,[10,11] and solitons.[12]

In recent years, in an effort to control low-frequency acoustic/elastic waves with compact and lightweight structures, researchers have explored a new kind of phase-modulated design known as metasurfaces.[13] A metasurface is a thin layer in the host medium composed of an array of subwavelength-scaled patterns, which can introduce an abrupt phase shift in the wave propagation path and tailor wavefront based on generalized Snell's law. By exploiting the phase modulation ability, researchers have proposed various metasurface designs to control the acoustic/elastic waves.[14–16] For example, the coiling-up space structure[14] and the Helmholtz-resonator[17] have been employed to control the acoustic wavefront of reflected and transmitted wave and realize various functions, e.g., wave deflecting and wave focusing. However, the existing metasurfaces mainly depend on linear behavior of

* These authors contributed equally. Further author information:
Zhenkun Lin: E-mail: zhenkunl@umich.edu
Yuning Zhang: E-mail: yuningz@umich.edu

Active and Passive Smart Structures and Integrated Systems XVI, edited by Jae-Hung Han
Shima Shahab, Jinkyu Yang, Proc. of SPIE Vol. 12043, 1204315
 · 0277-786X · doi: 10.1117/12.2612932

the structures. Recently, nonlinearity has been introduced in acoustic metasurface designs. For instance, Chen et.al.[18] presented a magnetic-control acoustic metasurface harnessing the nonlinearity of membrane structures to achieve tunable wavefront control through external magnetic stimulus. Later, Guo et.al.[19,20] explored nonlinear second-harmonic generation (SHG) in the spring-mass and rotating-square structures, and pointed out that SHG can be maximized when a larger non-zero resonance frequency doubles the lower one. Yet, they mainly focus on generating and maximizing the higher-order harmonics, while the phase modulation capability of the nonlinear structure are less explored. In addition, the resulting scattered wavefields often comprise a mixture of different harmonic components, which may weaken the efficiency to control them individually.

In this study, we propose a novel acoustic metasurface design with locally resonant nonlinear elements based on the curved beams. By tuning the masses of unit cells, different phase gradients are achieved to control the wavefront of the transmitted waves. The Harmonic Balance Method (HBM) is adopted to study the transmission characteristics of the acoustic waveguide along with numerical validation. With both analytical and numerical studies, we investigate its phase modulation and wavefront tailoring capability exploiting nonlinear effects. Accordingly, we design a nonlinear acoustic metasurface to control the wavefront of the transmitted wave under normally incident acoustic wave at a designed operating frequency of 1 kHz. We verify that the proposed nonlinear metasurface can generate significant second-harmonic component in the transmitted region. Simultaneously, we split the second-harmonic component from the fundamental frequency component by steering them into different directions. In addition, we propose a physical realization of the nonlinear acoustic metasurface with the nonlinear spring and lumped mass realized by spring steels and 3D-printed blocks, respectively.

The outline of this paper is as follows. In section 2, an analytical model of the acoustic waveguide is developed based on HBM to study its nonlinear transmission characteristics, along with numerical validation. In section 3, a nonlinear acoustic metasurface is introduced to realize simultaneous SHG and demultiplexing. Then, in section 4, we present a physical realization of the proposed concept. Section 5 summarizes the key points in this study.

## 2. MODELLING OF THE NONLINEAR ACOUSTIC WAVEGUIDE

### 2.1 Analytical formulation

The nonlinear metasurface proposed in this study is composed of an array of sub-wavelength unit cells, which consist of three lumped masses coupled via two curved beams, as shown in Fig. 1(**a**). Here, we consider the problem of acoustic wave transmission with normal incidence on the flat surface of the left lumped mass, $m_1$. To analytically characterize the wave propagation through the metasurface unit, we establish a simplified mass-spring-damper system, where we assume that the mass of the metasurface unit is all concentrated at the three lumped masses $m_1, m_2$, and $m_3$, and each curved beam is modelled as an ideal nonlinear spring with damping, as shown in Fig. 1(**b**).

Without loss of generality, the restoring forces of the nonlinear springs are assumed of the form, $F_i^{NL}(\Delta l) = k_i\Delta l + \alpha_i k_i \Delta l^2 + \beta_i k_i \Delta l^3, i = 1, 2$, where $k_i, \alpha_i$,and $\beta_i$ are the stiffness coefficients of the nonlinear springs and $\Delta l$ is the deformation of the nonlinear springs. Note that this cubic nonlinearity is often used for modelling the force-displacement relationships of curved beams.[8] We consider the acoustic propagation media to be air with mass density $\rho = 1.29\ kg/m^3$ and sound speed $c = 340\ m/s$, and assume longitudinal wave with plane stress-wave field $\sigma_{inc}(x,t) = \sigma_0 \sin(2\pi f(t - \frac{x}{c}))$ normally incident from the left hand side of the acoustic waveguide along positive $x$ direction, where $f$ and $\sigma_0$ are the frequency and amplitude of the incident wave, respectively. Assume that the resulting displacement field in the air is $u(x,t)$. Accordingly, the reflected and transmitted stress-wave fields can be given as follows.

$$\sigma_{ref} = \sigma_{inc} + \rho c \frac{\partial u}{\partial t}, \sigma_{tr} = -\rho c \frac{\partial u}{\partial t}, \tag{1}$$

where $\sigma_{ref}$ and $\sigma_{tr}$ represent the resulting reflected and transmitted stress-wave fields, respectively. Assume that the metasurface is located at $x = 0$ and its length is much less than the considered wave length. Then, the acoustic wave field should satisfy the boundary conditions on the metasurface at $x = 0$, i.e., $\sigma_{ref}|_{x=0} = \sigma_{inc}|_{x=0} + \rho c \frac{\partial u_1}{\partial t}$, and $\sigma_{tr}|_{x=0} = -\rho c \frac{\partial u_3}{\partial t}$, where $u_1$ and $u_3$ are the displacements of the lumped masses $m_1$ and $m_3$, respectively. Accordingly, the effective forces applied at $m_1$ and $m_3$ are: $F_1 = -(\sigma_{inc}|_{x=0} + \sigma_{ref}|_{x=0})S = -\big(2\sigma_0 \sin(2\pi f t) +$

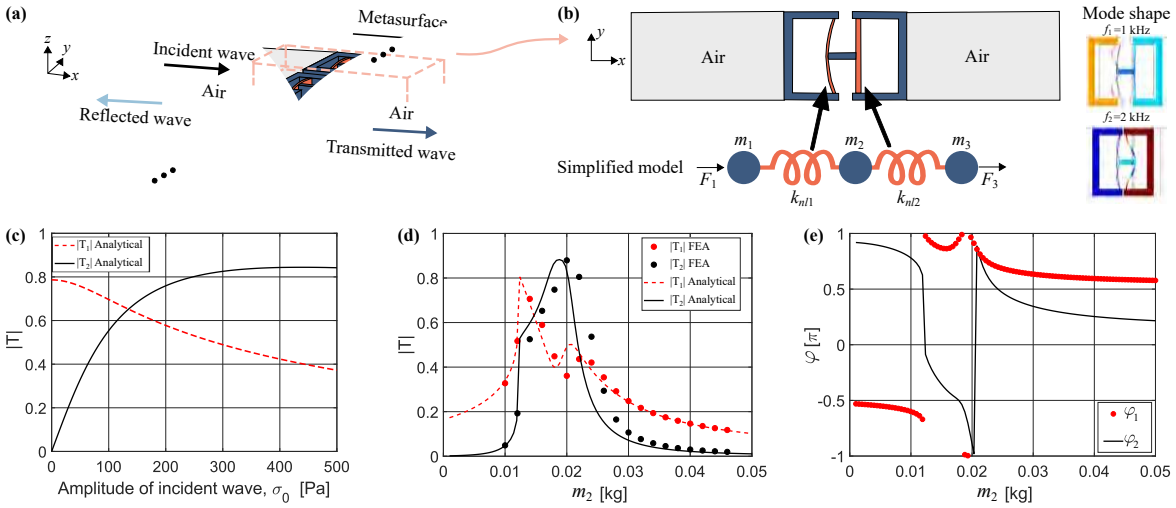


Figure 1. Schematic of the (**a**) nonlinear acoustic metasurface and (**b**) the one-dimensional waveguide. The inset in (**b**) demonstrates the mode shapes of the unit cell. (**c**) The transmission ratios of both fundamental component ($|T_1|$) and SHG ($|T_2|$) under different amplitudes of the incident wave. (**d**) The transmission ratios and (**e**) phase modulation curve of fundamental wave component ($\varphi_1$) and SHG ($\varphi_2$) under different $m_2$ value.

$\rho c\frac{du_1}{dt}\big)S$, and $F_3 = -\rho c\frac{du_3}{dt}$, where $S$ is the area of the flat surfaces contacting air. As such, the governing equations of the metasurface unit can be expressed as:

$$m_1\frac{d^2u_1}{dt^2} = -\big(2\sigma_0\sin(2\pi ft) + \rho c\frac{du_1}{dt}\big)S - F_1^{NL}(u_1-u_2) - \eta_1\frac{d(u_1-u_2)}{dt}, \tag{2a}$$

$$m_2\frac{d^2u_2}{dt^2} = F_1^{NL}(u_1-u_2) + \eta_1\frac{d(u_1-u_2)}{dt} - F_2^{NL}(u_2-u_3) - \eta_2\frac{d(u_2-u_3)}{dt}, \tag{2b}$$

$$m_3\frac{d^2u_3}{dt^2} = -\rho cS\frac{du_3}{dt} + F_2^{NL}(u_2-u_3) + \eta_2\frac{d(u_2-u_3)}{dt}, \tag{2c}$$

where $u_2$ is the displacement of $m_2$, and $\eta_1, \eta_2$ are the damping coefficients of the two nonlinear springs.

In the case of a harmonic incident wave, the equations of motion depicted in Eq. 2 can be analytically solved by using the HBM, where the solutions $u_i, i = 1, 2, 3$ are assumed in the form of a sum of all harmonics. That is, we have the following solution forms.

$$u_i(t) = u_i^0 + \sum_{n=1}^{N}\left[C_i^n\cos(2\pi nft) + S_i^n\sin(2\pi nft)\right], i = 1, 2, 3, \tag{3}$$

where $u_i^0$ represents the constant terms, $C_i^n$ and $S_i^n$ are the magnitudes of the sinusoidal terms cos and sin, respectively, and $N$ is the number of harmonics being considered. Substituting Eq. 3 into Eq. 2 and by matching the coefficients for different harmonics, we obtain a set of nonlinear equations about the unknowns $u_i^0$, $C_i^n$ and $S_i^n$, which can be numerically solved by Newton-Raphson Method.[21] With these solutions, we can obtain the complex transmission coefficients of each harmonic component by substituting Eq. 3 into Eq. 1, yielding:

$$T_n = \frac{2\pi nf\rho c}{\sigma_0}(C_i^n - jS_i^n),\ n = 1, 2, ..., N, \tag{4}$$

where $n$ indicates the $n-th$ order harmonics and $j$ is the imaginary unit. Then, the transmission ratio, $|T_n|$, of the $n-th$ order harmonics and its corresponding phase shift, $\varphi_n$, caused by the metasurface unit can be calculated by taking the magnitude and angle of $T_n$.

## 2.2 Results and validation

In the simplified unit cell model, we choose the parameters of the nonlinear springs, i.e., $k_i, \alpha_i$, and $\beta_i$, based on the force-displacement relationships of the curved beams obtained via quasi-static analysis in COMSOL

Multiphysics. The values of the rigid masses $m_1$, $m_2$ and $m_3$ are selected such that the resulting system will possess two linear resonance frequencies $f_1$ and $f_2$ with a relationship of $f_2 = 2f_1$. A more detailed description of structural parameters are shown in Table 1. Under such arrangement, the resonance frequencies of the unit cell are $f_2 = 2f_1 = 2$ kHz. The incident frequency is set to be $f = f_1 = 1$ kHz. It is recognized that with these two requirements satisfied, i.e., $f = f_1$ and $f_2 = 2f_1$, the SHG will be amplified by the resonance effects.[19,20]

Table 1. Parameters of the nonlinear metasurface unit cell with $f_2 = 2f_1 = 2$ kHz .

| Parameter | $m_1$ | $m_2$ | $m_3$ | $k_1$ | $k_2$ | $\alpha_1$ | $\alpha_2$ | $\beta_1$ | $\beta_2$ |
|---|---|---|---|---|---|---|---|---|---|
| Value | 9.4 $g$ | 20 $g$ | 6 $g$ | $3.0 \times 10^5$ N/m | $7.0 \times 10^5$ N/m | $-1823$ | 505.3 | $1.2 \times 10^6$ | $9.7 \times 10^5$ |

To characterize the effect of nonlinearity in the proposed metasurface unit, we first exam the influence of incident amplitude, $\sigma_0$, on the transmission coefficient, $T_n$. Figure 1(**c**) presents the analytical transmission ratios for the fundamental wave component, i.e., with frequency $f$, and the generated second-harmonic wave, i.e., with frequency $2f$, under different incident amplitudes, where the red dashed line represents the fundamental wave and the black solid line presents the SHG. We find that when the incident amplitude is nearly zero, there is only fundamental wave component in the transmitted wavefield, indicating nearly linear response. As the incident amplitude increases, the nonlinear effect occurs, leading to significant SHG. For large incident amplitude, e.g., above 150 Pa, the second-harmonic component even becomes stronger than the fundamental wave component, which demonstrates that the proposed metasurface provides a great platform for SHG. Note that, here, we do not plot all the other higher harmonic components ($n \geq 3$) since they are negligible compared with fundamental and second-harmonic components.

In addition, we also investigate how the transmitted wavefield can be tailored by tuning the structural design. Specifically, we change the value of $m_2$ by tuning the mass added to rigid block in the middle and obtain the transmission ratios and phase shifts of the fundamental and the second-harmonic components under different $m_2$, as shown in Fig. 1(**d**) and (**e**). We find that the tailoring of structural parameters such as $m_2$ will lead to dramatic change in the transmission ratio of both fundamental and second-harmonic components due to the change of local resonance. When $m_2 = 0.02$ kg, $f_2 = 2f_1 = 2$ kHz, and the SHG can be maximized as expected. Further, we observe different phase shifts for both fundamental and second-harmonic components by tailoring $m_2$, as shown in Fig. 1(**e**), which indicates the feasibility to achieve diverse phase gradient profiles for the metasurface design. It is important to note that the phase shift curve of the second-harmonic component covers the entire $[-\pi, \pi]$ phase range with different $m_2$, indicating that any type of anomalous wavefront control over the generated second-harmonic wave is achievable, while the phase shifts of the fundamental wave component remain almost unchanged within the region of interest. This interesting phenomenon offers us the possibility to control different harmonic components independently, and is used in our following metasurface design to split different frequency components.

To validate the simplified analytical model, we conduct the Finite Element Analysis (FEA) in COMSOL Multiphysics. Eigenfrequency analysis results show that the second non-zero resonance frequency doubles the first one as expected, $f_2 = 2f_1$. Also, we further explore the mode shape of two resonance frequencies of the unit cell as depicted in the inset of Fig. 1(**b**), which contains the information of the vibrating pattern at the resonance frequencies of the unit cell. Note that a large motion of $m_3$ can be identified in the second mode shape, indicating a significant SHG in the transmitted wavefield. Furthermore, we conduct time-domain numerical simulation of the acoustic waveguide with different $m_2$ value. The scattered acoustic pressure in the transmitted region is recorded, and then processed by the Fast Fourier transformation technique to obtain the transmission ratios of fundamental and the second-harmonic components and compared with analytical solutions as plotted in Fig. 1(**d**). The numerical transmission ratios agree well with the analytical results. Hence, the established simplified model can well characterize the scattered acoustic wavefield of the waveguide, which can be used to guide the following metasurface design.

## 3. METASURFACE DESIGN

### 3.1 Phase-modulated metasurface

The fundamental concept of the phase-modulated metasurface is to control the wavefront based on the generalized Snell's law by introducing an abrupt phase shift into the wave propagating path. Here, we design an acoustic metasurface to control the wavefront of the transmitted wave. Accordingly, the generalized Snell's law can be given as:

$$\frac{1}{2\pi}\frac{\mathrm{d}\varphi(y)}{\mathrm{d}y} = \frac{1}{\lambda_t}\sin\theta_t - \frac{1}{\lambda_i}\sin\theta_i, \tag{5}$$

where $\varphi(y)$ represents the abrupt phase shift introduced at location $y$. $\theta_t$ ($\theta_i$) and $\lambda_t$ ($\lambda_i$) are the angle and wavenumber of the transmitted (incident) wave, respectively. By tailoring the phase profile along the metasurface, we can control the wavefront and achieve desired wave functions.

### 3.2 Metasurface design for simultaneous SHG and demultiplexing

In this section, we present a nonlinear acoustic metasurface design for simultaneous higher-harmonic generation and demultiplexing. Specifically, we design a nonlinear acoustic metasurface composed of an array of 25 units with a unit gap of 2 mm to control the normally incident acoustic wave at 1 kHz. The finite element model of the entire nonlinear acoustic metasurface is established in COMSOL multiphysics as depicted in Fig. 2(**a**), where the propagating medium is air and the perfectly matched layers (PMLs) surrounding the system are established to avoid the reflection from the boundary and simulate the infinite acoustic domain. Due to the nonlinearity and the linearized resonance of the system ($f_2 = 2f_1$), significant SHG can be identified in the transmitted wavefield. By tailoring the mass value $m_2$ along the metasurface, the metasurface can guide the generated second-harmonic wave in any desired angle, while the propagating direction of the fundamental wave remains unchanged according to the phase modulation feature discussed in Section 2.2.

To guide the $f_2$ component propagate at an angle $\theta_2$ in the transmitted region under normal incidence, the phase gradient profile of $f_2$ component $\varphi_2(y)$ should satisfy Eq. 6 according to the generalized Snell's law.

$$\varphi_2(y) = \frac{2\pi y}{\lambda_2}\sin\theta_2, \tag{6}$$

where $\lambda_2$ is the wavelength of the second-harmonic component.

To this end, we design a metasurface with a theoretical deflecting angle of $\theta_2 = 60^\circ$ for the second-harmonic wave, while the fundamental wave component will remain in the same propagating direction, i.e., $\theta_1 = 0^\circ$, based on the phase gradient profile depicted in Fig. 2(**b**) and (**c**). The phase gradient profile of the SHG shows a linear pattern for desired transmitted angle $\theta_2 = 60^\circ$. On the other hand, most of the units introduce an constant phase shift $\varphi_1(y) \approx \pi$ to the fundamental wave, indicating the same transmitted angle as the incident wave $\theta_1 = 0^\circ$. Accordingly, the required $m_2$ profile are obtained as plotted in Fig. 2(**d**). Note that we can easily change the $m_2$ value through adding/subtracting additional mass unit in the engineering practice, which enables an adaptive nonlinear metasurface design for broadband frequency wave control.

Accordingly, the frequency domain simulation is conducted in COMSOL Multiphysics to test the performance of the nonlinear metasurface. Figure 2(**e**) shows the shows the resulting scattered acoustic pressure field. It can be identified that the nonlinear acoustic metasurface can realize significant SHG in the transmitted wavefield. Also, the incident wave is split into two beams after being scattered by the nonlinear metasurface, one in the original propagating direction with the same wavelength as the incident wave $\theta_1 = 0^\circ$ (i.e., the fundamental wave component) and the other one being deflected by 60 degrees with half of the original wavelength $\theta_2 = 60^\circ$ (i.e., the second-harmonic component). Hence, the numerical results validate that the proposed nonlinear acoustic metasurface can achieve simultaneous SHG and demultiplexing.

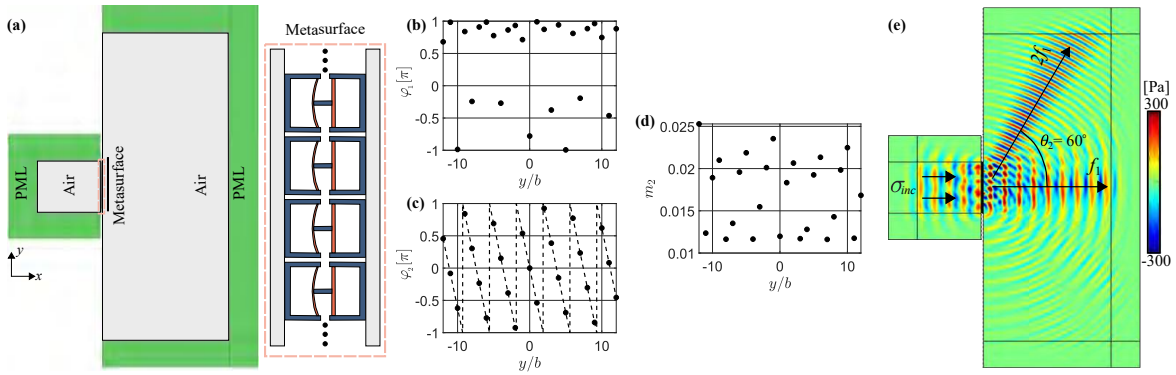


Figure 2. (**a**) Schematic of the nonlinear acoustic metasurface. The surrounded PMLs are established to mimic infinite acoustic domain. (**b,c**) The phase gradient profiles of the (**b**) fundamental and (**c**) SHG. (**d**) The corresponding $m_2$ profile with the coordinate origin (y=0) locating at the midpoint of the metasurface. b=52.8 mm represents the distance between adjacent units. (**e**) The scattered acoustic wavefields verifying simultaneous higher-harmonic generation and demultiplexing.

## 4. EXPERIMENTAL CONFIGURATION

The prime focus of this section is to physically realize the proposed nonlinear metasurface design. The curved beams made of 1095 spring steel (McMaster-Carr) is used to achieve the nonlinear effect. The mass units $m_1$, $m_2$ and $m_3$ are obtained through Form 3 SLA 3D Printer. The nonlinear stiffness of the spring steel is tested through Instron Tensile Testing Machines as pictured in Fig. 3(**a**). Figure 3(**b**) shows the measured nonlinear stiffness of a curved spring steel which performs as expected. The desired nonlinearity of the nonlinear spring, $k_{nl1}$ and $k_{nl2}$ can be achieved by tailoring the length, thickness and bending angle of the spring steels. Next, 3D-printed mass blocks are connected through the spring steels creating the unit cells that are hung with twine as shown in Fig. 3(**c**). Accordingly, the entire nonlinear acoustic metasurface can be constructed by periodically placing the units. By adding additional mass on $m_2$ blocks and tailoring the phase gradient, the entire metasurface is promising to achieve simultaneous SHG and demultiplexing as demonstrated in the analytical and numerical studies.

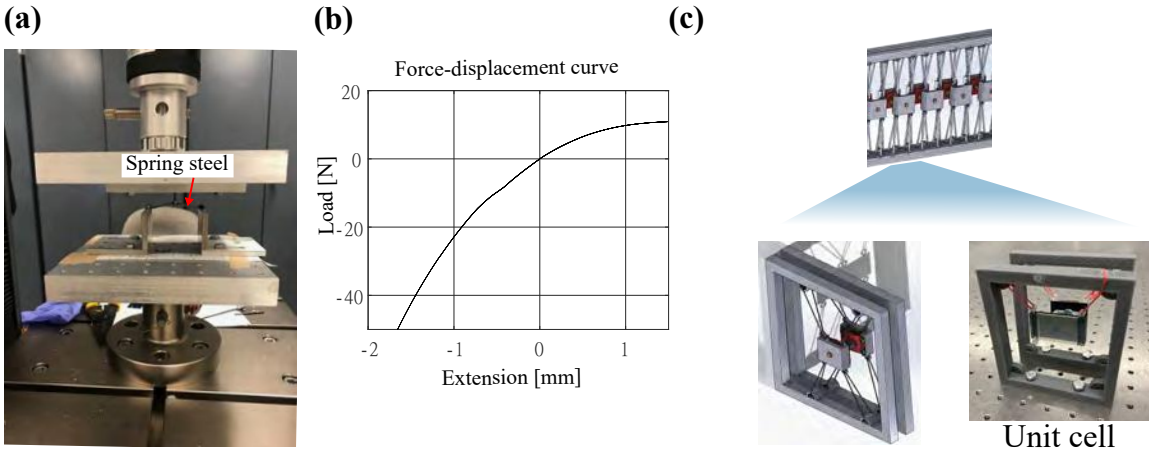


Figure 3. (**a**) Tensile testing of spring steel. (**b**) Force-displacement curve of the spring steel. (**c**) Schematic of the nonlinear acoustic metasurface and its unit cell.

## 5. CONCLUSION

In this paper, we explore a novel acoustic metasurface design with locally resonant nonlinear elements based on curved beams. By exploiting the nonlinearity in the curved structure, we investigate the nonlinear phenomenon,

specifically SHG, of the proposed system using both analytical and numerical methods. The SHG is amplified by setting the second non-zero resonance frequency to be twice of the first one. Also, an analytical formulation of the acoustic waveguide is developed and validated through numerical results, verifying a significant SHG in the transmitted wavefield. By tailoring the structural parameters of the unit cell, specifically mass $m_2$, different phase gradients are achieved in the transmitted fundamental and second-harmonic components. Our results show that the phase modulation curve of the SHG covers the entire $2\pi$ phase range while the phase shift of the fundamental wave is limited in a small range, which is further exploited for demultiplexing metasurface design. To this end, we propose a nonlinear metasurface design which is capable of generating higher-order harmonic in the transmitted wavefield and simultaneously splitting different frequency components by steering them into different directions, i.e., realizing frequency demultiplexing. Finally, we present an actual physical realization of the nonlinear acoustic metasurface, and its experimental validations are currently underway. Overall, the nonlinear acoustic metasurface offers a novel avenue to harness nonlinear effects for acoustic wavefront tailoring and develops new potentials towards more efficient technologies for wave-based engineering applications such as acoustic/elastic lenses, acoustic diodes, and signal processing and identification systems.

## ACKNOWLEDGMENTS

This work was supported by the National Science Foundation under Grant No. CMMI-1933436 and the Air Force Office of Scientific Research under Grant FA9550-21-1-0032.

## REFERENCES

[1] Hussein, M. I., Leamy, M. J., and Ruzzene, M., "Dynamics of phononic materials and structures: Historical origins, recent progress, and future outlook," *Applied Mechanics Reviews* **66**(4) (2014).

[2] Ma, G. and Sheng, P., "Acoustic metamaterials: From local resonances to broad horizons," *Science advances* **2**(2), e1501595 (2016).

[3] Tol, S., Degertekin, F. L., and Erturk, A., "Phononic crystal luneburg lens for omnidirectional elastic wave focusing and energy harvesting," *Applied Physics Letters* **111**(1), 013503 (2017).

[4] Hu, G., Tang, L., Liang, J., Lan, C., and Das, R., "Acoustic-elastic metamaterials and phononic crystals for energy harvesting: A review," *Smart Materials and Structures* (2021).

[5] Barnhart, M. V., Xu, X., Chen, Y., Zhang, S., Song, J., and Huang, G., "Experimental demonstration of a dissipative multi-resonator metamaterial for broadband elastic wave attenuation," *Journal of Sound and Vibration* **438**, 1–12 (2019).

[6] Lin, Z., Al Ba'ba'a, H., and Tol, S., "Piezoelectric metastructures for simultaneous broadband energy harvesting and vibration suppression of traveling waves," *Smart Materials and Structures* **30**(7), 075037 (2021).

[7] Dorin, P. and Wang, K. W., "Broadband frequency and spatial on-demand tailoring of topological wave propagation harnessing piezoelectric metamaterials," *Frontiers in Materials* , 409 (2021).

[8] Wu, Z., Zheng, Y., and Wang, K. W., "Metastable modular metastructures for on-demand reconfiguration of band structures and nonreciprocal wave propagation," *Physical Review E* **97**(2), 022209 (2018).

[9] Wu, Z. and Wang, K. W., "On the wave propagation analysis and supratransmission prediction of a metastable modular metastructure for non-reciprocal energy transmission," *Journal of Sound and Vibration* **458**, 389–406 (2019).

[10] Boechler, N., Theocharis, G., and Daraio, C., "Bifurcation-based acoustic switching and rectification," *Nature materials* **10**(9), 665–668 (2011).

[11] Popa, B. I. and Cummer, S. A., "Non-reciprocal and highly nonlinear active acoustic metamaterials," *Nature communications* **5**(1), 1–5 (2014).

[12] Sugimoto, N., Masuda, M., Ohno, J., and Motoi, D., "Experimental demonstration of generation and propagation of acoustic solitary waves in an air-filled tube," *Physical Review Letters* **83**, 4053–4056 (1999).

[13] Assouar, B., Liang, B., Wu, Y., Li, Y., Cheng, J. C., and Jing, Y., "Acoustic metasurfaces," *Nature Reviews Materials* **3**(12), 460–472 (2018).

[14] Li, Y., Jiang, X., Li, R. Q., Liang, B., Zou, X. Y., Yin, L. L., and Cheng, J. C., "Experimental realization of full control of reflected waves with subwavelength acoustic metasurfaces," *Physical Review Applied* **2**, 064002 (2014).

[15] Cummer, S. A., Christensen, J., and Alù, A., "Controlling sound with acoustic metamaterials," *Nature Reviews Materials* **1**(3), 1–13 (2016).

[16] Lin, Z. and Tol, S., "Elastic metasurfaces for full wavefront control and low-frequency energy harvesting," *Journal of Vibration and Acoustics* **143**(6), 061005 (2021).

[17] Lan, J., Li, Y., Xu, Y., and Liu, X., "Manipulation of acoustic wavefront by gradient metasurface based on helmholtz resonators," *Scientific reports* **7**(1), 1–9 (2017).

[18] Chen, X., Liu, P., Hou, Z., and Pei, Y., "Magnetic-control multifunctional acoustic metasurface for reflected wave manipulation at deep subwavelength scale," *Scientific reports* **7**(1), 1–9 (2017).

[19] Guo, X., Gusev, V. E., Bertoldi, K., and Tournat, V., "Manipulating acoustic wave reflection by a nonlinear elastic metasurface," *Journal of Applied Physics* **123**(12), 124901 (2018).

[20] Guo, X., Gusev, V. E., Tournat, V., Deng, B., and Bertoldi, K., "Frequency-doubling effect in acoustic reflection by a nonlinear, architected rotating-square metasurface," *Physical Review E* **99**(5), 052209 (2019).

[21] Ypma, T. J., "Historical development of the newton–raphson method," *SIAM review* **37**(4), 531–551 (1995).